

Modeling Metallic Halide Local Structures in Salt Melts Using a Genetic Algorithm

Matthew S. Christian, Timothy J. Lynch, Juliano Schorne-Pinto, Amir M. Mofrad, Nancy R. Birkner, Kyle S. Brinkman, Wilson K. S. Chiu, and Theodore M. Besmann*



Cite This: <https://doi.org/10.1021/acs.jpcc.2c00747>



Read Online

ACCESS |



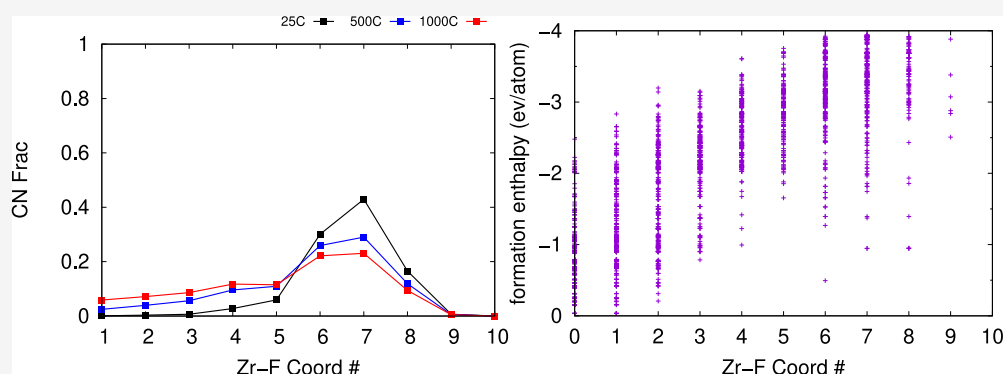
Metrics & More



Article Recommendations



Supporting Information



ABSTRACT: Knowing the local structure of metal ions in molten salt melts is essential for understanding the chemistry related to corrosion and solvation processes for various applications such as molten salt reactors, solar thermal power systems, and molten salt-enabled materials processing. However, modeling the dynamic local structure of metals in salt melts is difficult because classical mechanics does not reproduce the correct local atomic networking. The computational cost of carrying out multiple first-principles dynamics calculations to ensure that the compositional space is well sampled can be prohibitively large. In order to address this issue, the current study explores the use of the evolutionary algorithm Universal Structure Predictor: Evolutionary Xtallography (USPEX) to predict coordination numbers of strontium and zirconium in binary and ternary chloride and fluoride melts. Temperature-dependent coordination number distributions for the metal atoms were computed using a Boltzmann distribution. The calculated average coordination numbers were found to be consistent with observations from extended X-ray absorption fine structure (EXAFS) experiments and the expected temperature trends. Furthermore, the most stable predicted crystal structures compare well with EXAFS values, validating our approach for predicting local structures in salt melts.

1. INTRODUCTION

Understanding the local structure of metal ions in salt melts is important for monitoring the species present in the system, particularly for monitoring corrosion in molten salt reactors and solar thermal power systems.^{1,2} In addition, since metals can have multiple coordination environments that depend on the concentration, oxidation state, and temperature,³ knowing the metal coordination in a salt melt can also be beneficial for developing in situ system monitors for salt melts.

It is possible to determine the local coordination of metals experimentally. Previous research has used nuclear magnetic resonance (NMR) spectroscopy,^{4–6} Raman spectroscopy,⁷ and X-ray absorption spectroscopy (XAS)^{8,9} to study metal coordination. These experiments are established for systems with singular coordination environments or oxidation states. Still, they can be challenging for metals with multiple oxidation states and coordination environments.^{3,10} Computational investigations can be used to decipher experimental inves-

tigations, providing a decomposition of the multiple coordination environments.^{6,8,11–13}

Molecular dynamics (MD) calculations coupled with XAS investigations have been frequently used to determine coordination states in salt melts.^{10–12,14} However, both classical MD potentials and density functional theory (DFT)-based methods have potential issues when modeling actinide salts. For example, classical potentials may not capture the complex interactions between actinide metals and typically do not describe the proper ordering that occurs in ionic liquids. These interactions can be captured via ab initio MD (AIMD)

Received: January 30, 2022

Revised: May 18, 2022

simulations but carrying out the number of calculations required to adequately sample the compositional space is quite expensive. Using a stochastic generator for salt compositions coupled with DFT could provide an equally accurate alternative to carrying out multiple AIMD calculations to predict temperature and compositional-dependent coordination environments while reducing computational time.

The Universal Structure Predictor: Evolutionary Xtallography (USPEX) algorithm^{15,16} is a genetic algorithm used for predicting crystal structures from user-defined elements based on a library of space groups. Each hypothetical crystal structure undergoes structural optimization via DFT, and USPEX generates a thermodynamic convex hull from the crystal structure set. Crystal structures with energies closest to the thermodynamic convex hull are permuted to create the next generation, with the cycle continuing until a convergence criterion has been met. USPEX has been used previously in the study of uranium oxides¹⁷ and silicates,¹⁸ as well as perovskites^{19,20} and high-entropy alloys.²¹ Though these applications are for solids, USPEX has been used for analyzing atom clusters in various applications, including liquids.^{22–27}

This work uses the USPEX algorithm to analyze the coordination of strontium in a SrCl₂–NaCl melt and zirconium in a ZrF₄–LiF melt that have been previously experimentally investigated using both Raman spectroscopy and extended X-ray absorption fine structure (EXAFS) spectroscopy,²⁸ and Boltzmann weighted probability distributions for coordination numbers (CNs) are generated from the USPEX data and compared to the experimental values. This approach assumes that the local environment in USPEX's generated crystal structures is the same as or similar to the local structure of the metals in the salt melt. Our approach is justified by the apparent agreement between the average computed CNs and the most stable predicted crystal structures from EXAFS observations.

2. COMPUTATIONAL METHODS

2.1. Genetic Algorithm for Structural Prediction.

Crystal structures for Sr–Cl, Sr–Na–Cl, Zr–F, and Zr–Li–F elemental combinations were generated using USPEX version 9.4.4.¹⁵ Elemental binary systems were limited to 20 atoms, while ternary systems had up to 40 atoms per generated crystal structure. Each calculation began with the generation of 100 random crystal structures of varying crystal volumes and space groups that were then evaluated using the Vienna ab initio simulation package (VASP) electronic structure package. After finishing the initial calculations, the 60 lowest energy crystal structures from the initial calculations were used as input to generate new crystal structures. New crystal structure generations were created using USPEX with the following perturbation operations: 40% heredity (offspring produced via random splicing of crystal cells), 20% soft mutation (atomic displacements generated along the softest phonon mode), 10% lattice mutation (permutation of lattice constants), and 10% transmutation (translation of atoms through the unit cell). Additionally, 20% new random crystal structures were added to each generation. Each offspring generation contained 50 crystal structures, and the cycle of producing new hypothetical crystals was carried out for 40 generations. Although USPEX includes a semiempirical method to include thermal effects to rank structures, the algorithm was set to rank structures on 0 K DFT enthalpy. Therefore, it is expected that high-temperature structures that are stabilized by phonon vibrations are likely to

not be predicted using USPEX. This process generated a data set of 1000–1200 atom configurations per element combination to represent a stochastic sampling representing a liquid.

2.2. Structural Optimization Process. A series of DFT calculations were carried out for each crystal structure in order to ensure that it had reached its lowest energetic state before being evaluated by the USPEX algorithm. Each calculation used the projector-augmented wave²⁹ approach as implemented in the VASP^{30–33} electronic structure program using the Perdew–Burke–Ernzerhof exchange–correlation functional.³⁴ This functional was chosen because of its proven ability to accurately model uranium compounds.^{35,36} “Cold” smearing³⁷ was used with a parameter of 0.02 eV and a wavefunction cutoff of 600 eV. van der Waals interactions were incorporated into the calculations through Grimme's DFT-D3 correction,³⁸ a requirement to accurately calculate enthalpies and structures for uranium chlorides.^{39,40} Convergence criteria for the total energy was set to 1×10^{-4} eV, and forces were set to 1×10^{-4} eV/Å. Three total calculations were carried out with successively higher *k*-point meshes. The first two were structural optimizations with *k*-point spacings of 0.25 and 0.15 Å⁻¹. Finally, a single-point calculation with a 0.08 Å⁻¹ *k*-point spacing was used to evaluate the relative stability using USPEX for each crystal structure.

After the USPEX algorithm completed the run, a final DFT single-point calculation was carried out for each USPEX generated crystal structure in order to provide data as an input for calculating the temperature-dependent CN distribution, using the same parameters as those for the USPEX calculations, but instead using an automatic generated *k*-point mesh with 50 *k*-points per side.

2.3. Calculation of Temperature-Dependent CN Distributions. Zr–F and Sr–Cl CNs were extracted from each USPEX generated crystal structure using the CRITIC2 package.⁴¹ Our measure of crystal stability for this study is crystal formation enthalpy, which was calculated using Open Quantum Materials Database (OQMD) atomic potentials.⁴² It is known that the CNs for these systems can depend on both the composition and temperature, but DFT inherently models systems at 0 K. Typically, temperature effects would be included via vibrational phonon calculations, but carrying out such calculations for all USPEX generated crystals is cost prohibitive. Instead, temperature effects are accounted for by using the Boltzmann probability. Our probability formulation is based on how coordinating species can stabilize a central atom.^{43–47} This change in energy is reflected in the per-atom formation enthalpy of a compound or a cluster. The probability, P_i , of a metal atom *i* having any CN in a structure with per-atom formation enthalpy E_i is

$$P_i(\text{CN}) = \frac{e^{-E_i/k_B T}}{\sum_j e^{-E_j/k_B T}} \quad (1)$$

where T is the temperature in Kelvin, k_B is the Boltzmann constant, and E_j is the per-atom formation enthalpy for the set of the metal center structure. The total probability of a metal having a given CN, $P(\text{CN})$, is obtained by summing the probability of all CN states, $P_i(\text{CN})$

$$P(\text{CN}) = \sum_i P_i(\text{CN}) \quad (2)$$

2.4. Experimental Agreement. The results of this computational study are paired with the experimental

investigations carried out by Lynch et al.,²⁸ who investigated melts containing 5 mol % SrCl₂ in NaCl and 5 mol % ZrF₄ in LiF. The most stable structures identified using USPEX were used as input for structural fits to EXAFS measurements.

The XAS data were first processed using the Athena package of Demeter,⁴⁸ where spectra were normalized and the background was removed by fitting a spline to the EXAFS part of the absorption data. The Fourier transform from the frequency domain (*k*-space) to the R-space was carried out using a Hanning window, and the Fourier transform parameters were chosen depending on *k*-space data quality. The results of these operations were then fitted in the Artemis package of Demeter from 25 to 1100 °C in approximately 200 °C increments. The number of scattering paths used for fitting was tested for their statistical significance using a Hamilton F-test.^{49,50} Processed data from Athena were compared to FEFF calculations determined in Artemis from USPEX generated structures. Scattering paths were chosen based on the scattering type (only single scattering was considered) as well as the expected bond lengths.^{8,51} The determined parameters were the amplitude reduction factor S_0^2 , the offset of the absorption peak energy of the data and ΔE_0 , the disorder parameter that factors in the thermal and static disorder σ^2 , the bond distances between atoms *R*, and the CN *N*. Accuracy of the fit is determined by the degree of deviation from the original EXAFS results, where the accuracy of the structure is inversely proportional to the deviation of the curves.

3. RESULTS

3.1. Sr–Cl and Zr–F Calculations. Before using USPEX to model the SrCl₂–NaCl and ZrF₄–LiF melt systems, the accuracy was first tested by carrying out calculations on the simpler Sr–Cl and Zr–F binary systems with the predicted thermodynamic convex hull crystal stoichiometries listed in Table 1. USPEX largely predicts the correct binary salt and

Table 1. Experimental and USPEX-Predicted Sr–Cl and Zr–F Crystal Structure Stoichiometry

Sr–Cl		Zr–F	
USPEX	expt.	USPEX	expt.
Sr ₂₉	Sr ₄	Zr ₁₂	Zr ₂
Cl ₈	Cl ₈	F ₁₂	F ₈
Sr ₄ Cl ₈	Sr ₄ Cl ₈	Zr ₂ F ₈	Zr ₈ F ₃₂

elemental chlorine stoichiometries. However, it fails to predict the correct stoichiometry for elemental fluorine and metallic crystal structures. It likely did not predict the proper ZrF₄ analogue because the computed crystal structures were limited to 20 atoms and experimentally known crystals contain 30 and 40 atoms per unit cell, respectively.^{52,53} Although USPEX did not predict the correct crystal structures as lying along the thermodynamic convex hull, the correct crystal structures were found to be within 0.1 eV/atom of the convex hull, suggesting that not fully including crystal vibrational effects may have influenced the USPEX-derived crystal structure ranking.

The temperature-dependent CN distribution is shown in Figure 1. At room temperature, Sr prefers 6-, 7-, or 8-coordinate structures with chlorine, having an average CN of 6.61. This differs from the experimental SrCl₂, which crystallizes in the fluorite structure with CN = 8. Zr–F is similar to Sr–Cl but with a greater preference for 7-coordinate

structures, having an average CN of 6.8 compared to an experimental value of 8. As the temperature increases, the probability of having smaller CNs increases such that the probability of having CN = 5 is non-negligible, shifting the average CN to 5.5 at 500 °C and 4.88 at 1000 °C. The probability of Zr having CN = 6 is slightly less than that for CN = 7, shifting the average CN to 6.20 at 500 °C and 5.77 at 1000 °C. This is because the crystal formation enthalpy is proportional to the CN in our method, and as the temperature increases, the Boltzmann probability of being in a higher-energy, lower-coordinated state increases. The results in Figure 1 also show a compositional dependence on the CN, which has previously been seen experimentally.^{8,14,54}

3.2. Sr–Na–Cl and Zr–Li–F Calculations. While USPEX calculations were not able to fully predict the correct experimentally observed crystal structures, their ability to correctly predict known stoichiometric ratios and compositional trends encouraged efforts to examine ternary compositions.

A comparison of USPEX-predicted Sr–Na–Cl and Zr–Li–F ternary system stoichiometry with known experimental compositions is seen in Table 2. Like the binary salt systems, USPEX failed to predict the correct pure elemental structures, and computed stoichiometries are much larger than those experimentally known. However, the algorithm correctly predicted the absence of Sr–Na–Cl ternaries and the correct ratios for two Li–Zr–F ternaries. It is expected that USPEX did not predict the observed Li₃ZrF₇ ternary crystal structure because it forms at >740 K.⁵⁵

Temperature-dependent coordination distributions for the ternary systems are similar to our binary system results. Our Sr–Na–Cl calculations show a maximum probability of CN = 7 but has a calculated average of CN = 6.04. However, the ternary calculations have a lower probability of CN = 8 and a higher probability of CN = 4 and 5 than the Sr–Cl binary calculations. The probability of CN = 6 and 7 equalizes at 500 °C, reducing the average CN to 4.98. At 1000 °C, there is an equal probability of Sr to have CN = 0 to 7, further lowering the average CN to 4.38. This is likely because the USPEX algorithm could not predict a stable ternary structure and therefore generated multiple crystal structures with varying CNs but with near-equal formation enthalpies.

At room temperature, the Zr CN probability is 42% for CN = 7, 30% for CN = 6, and 17% for CN = 8, resulting in an average CN of 6.63. Upon increasing the temperature to 500 °C, the probabilities of CN = 7 and CN = 6 reduce to 29 and 26%, respectively, while the probability of CN = 5 increases to 11%. This reduces the average CN to 5.79. Increasing the temperature to 1000 °C decreases CN = 7 to 23% and CN = 6 to 22% while increasing CN = 4 and CN = 5–11%, lowering the average CN to 5.24.

Like the binary calculations, CN is dependent on the metal composition (see the Supporting Information). Although low CNs can be present at low metal fractions (less than 40% metal composition), the compositions have a high alkali fraction, which compete with the metal to coordinate with the halogen atom. Formation enthalpies for these compounds show that the energy landscape is flat for Sr–Na–Cl crystal structures with CN = 4–8 (Figure 2e). However, many Sr–Na–Cl crystal structures with CN = 0–3 are only slightly less stable than those with CN = 4–8, having a formation enthalpy between –2.0 and –2.5 eV. Formation enthalpies for Zr–Li–F crystal structures are the greatest for CN = 6–8, but there is

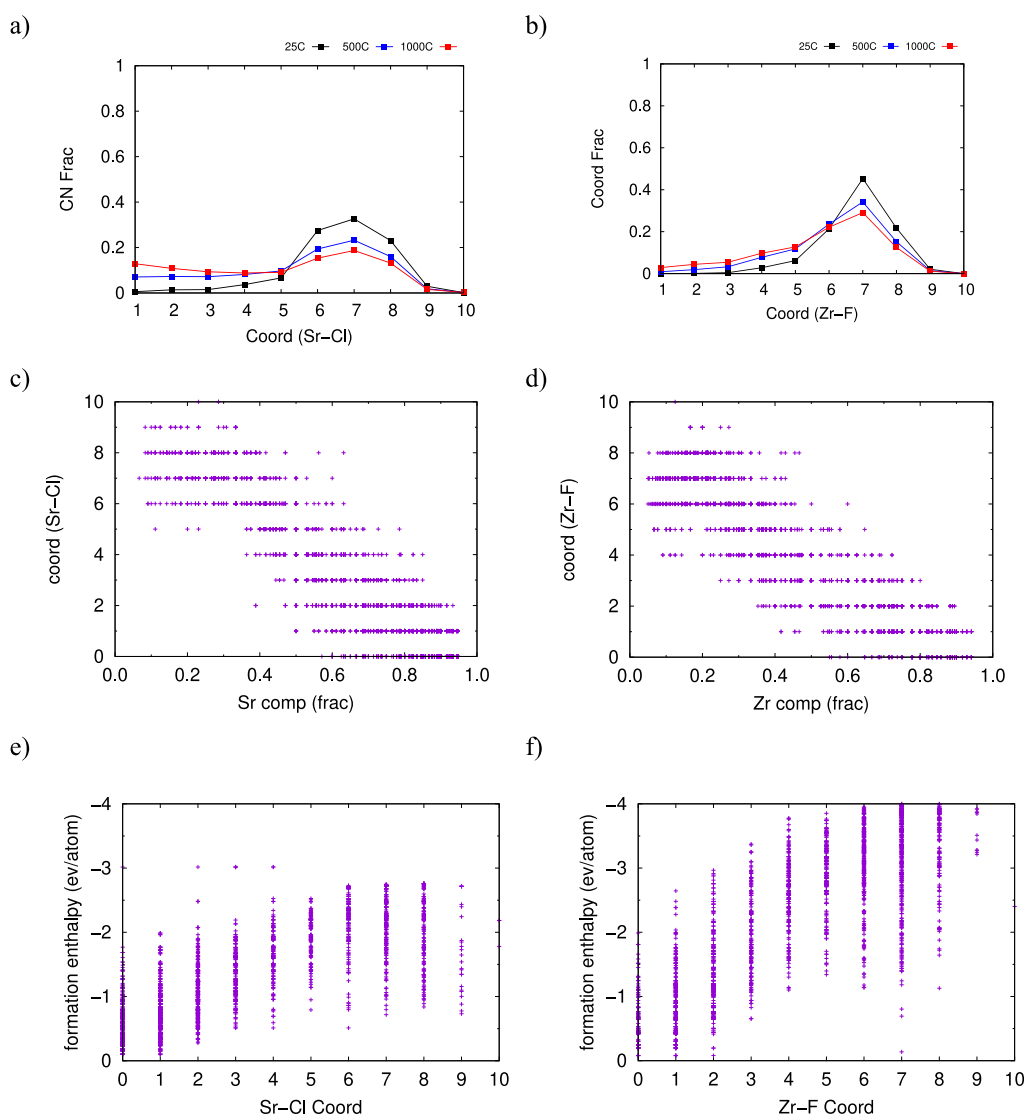


Figure 1. Results for Sr–Cl and Zr–F calculations: (a,b) temperature-dependent CN distributions for three different temperatures, (c) Sr–Cl CN as a function of the Sr atom fraction, (d) Zr–F CN as a function of the Zr atom fraction, and (e,f) CNs as a function of the formation enthalpy in electronvolts per atom.

Table 2. Experimental and USPEX-Predicted Sr–Na–Cl and Zr–Li–F Crystal Structure Stoichiometry

Sr–Na–Cl		Zr–Li–F	
USPEX	expt.	USPEX	expt.
Sr ₂₄	Sr ₄	Zr ₁₂	Zr ₂
Na ₂₀	Na ₉	Li ₃₇	Li ₄
Cl ₃₆	Cl ₈	F ₁₂	F ₈
Na ₇ Cl ₇	Na ₄ Cl ₄	Li ₁₂ F ₁₂	Li ₁₄ F ₄
Sr ₃ Cl ₆	Sr ₄ Cl ₈	Zr ₂ F ₈	Zr ₈ F ₃₂
		Li ₁₆ Zr ₈ F ₃₈	Li ₁₆ Zr ₈ F ₃₈
		Li ₈ Zr ₄ F ₂₄	Li ₈ Zr ₄ F ₂₄
		Li ₃ ZrF ₇	

also a greater frequency of these crystal structures, resulting in a larger CN distribution probability.

3.3. Experimental Validation Using EXAFS. XAS experiments that measured Sr and Zr CNs in chloride and fluoride salt melts have previously been performed for 5 mol % ZrF₄ in LiF and 5 mol % SrCl₂ in NaCl.²⁸ In order to directly compare our calculations to these experiments, the data set was

narrowed down to only contain crystal structures that contained <10% atom fraction of Sr and Zr. The CN distribution of this narrowed data set, with arrows indicating experimental XAS measured CNs, are shown in Figure 3.

Table 3 shows that the USPEX-calculated average CN is within the experimental uncertainty and that CN decreases as temperature increases. At room temperature, our Sr–Na–Cl calculations show a distribution of CN = 6 and 7, while pure SrCl₂ is known to have CN = 8. This disagreement is likely because our model aims to model the probability of CNs in liquids, not in solids. Therefore, agreement between calculations and experiments increases as temperature increases, being nearly the same at 1000 °C, having a calculated average CN of 5.6 compared to an experimentally measured CN of 5.8.

The CN distribution for Zr–Li–F is narrower than that of Sr–Na–Cl, favoring CN = 7 with a probability of 61% and probabilities of CN = 6 and 8 both equal to 18%. At increased temperatures, CN = 7 and 8 probability decreases while that of CN = 6 increases. At 600 °C, the average calculated CN is nearly equal to the experimental value (6.3 compared to 6.2) but is greater than the experimental value at 1000 °C (6.1 vs

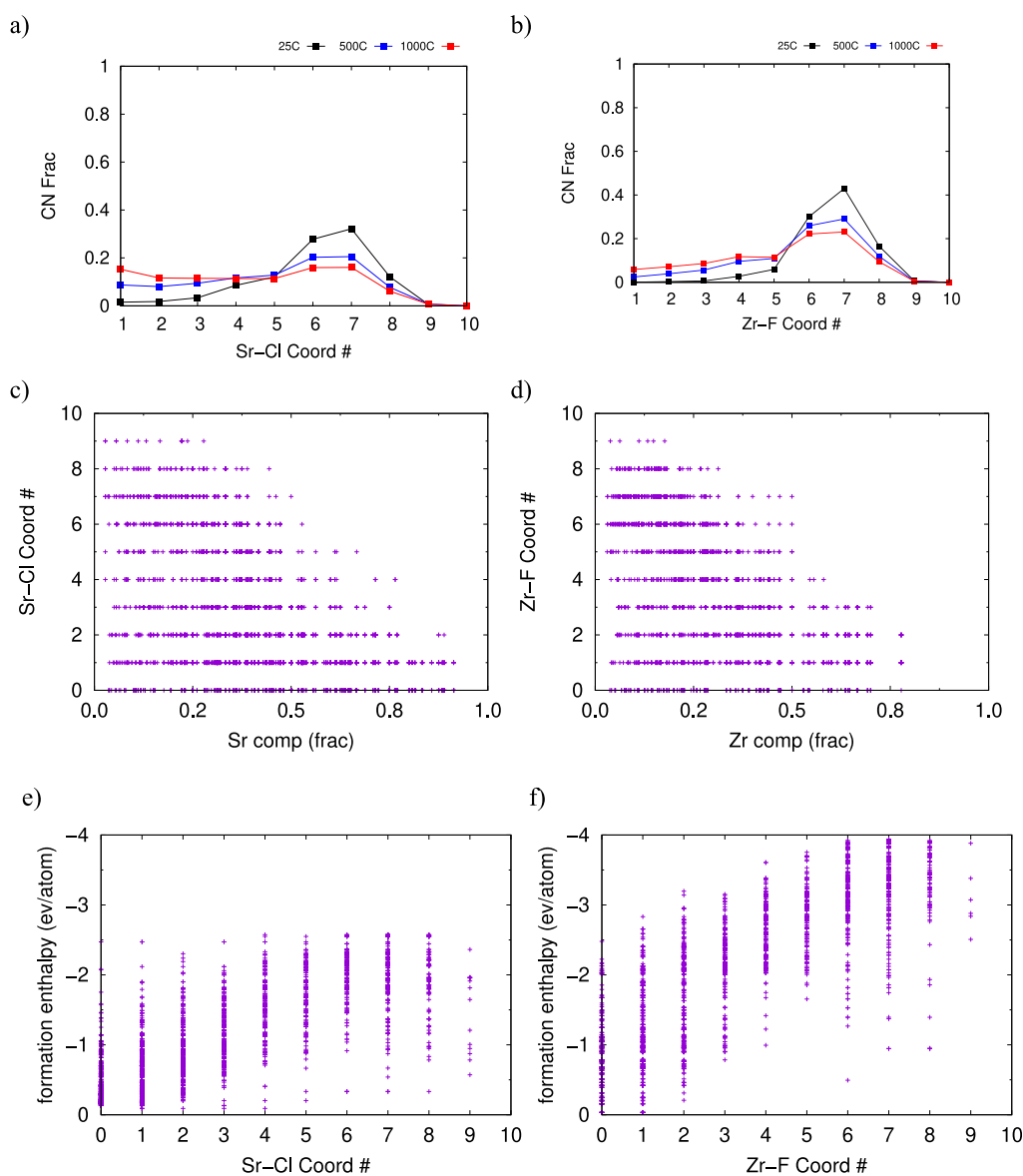


Figure 2. Results of Sr–Na–Cl and Zr–Li–F calculations: (a,b) CN distributions for three different temperatures; (c) Sr CN as a function of the Sr atom fraction; (d) Zr CN as a function of the Zr atom fraction; and (e,f) CN values as a function of formation enthalpies.

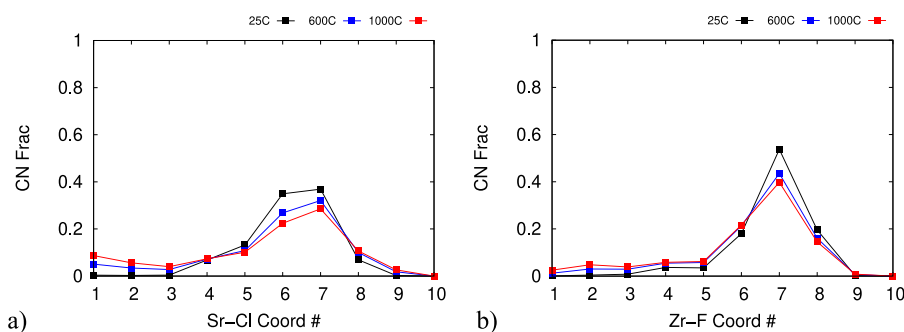


Figure 3. CN distribution for 10% maximum metal composition for Sr–Na–Cl (a) and Zr–Li–F (b).

4.5). This is likely due to the scattering by Zr in the melt. This difference may be caused by the presence of multiple Zr–F complexes in the molten salt (ZrF_6^{2-} , ZrF_7^{3-} , and ZrF_8^{4-}), resulting in a convoluted averaged spectrum that can be distorted due to interference by the individual complexes.^{8,14}

Further validation of our calculations was carried out by using the most stable ternary crystal structures to fit the 400 and 1000 °C XAS data for each salt (Figure 4). As stated, raw XAS data were first processed in the Athena package. The processed XAS data from Athena were then fitted for XAS parameters using the USPEX-generated structure in Artemis.

Table 3. Experimental and Modeled CNs for SrCl₂–NaCl and ZrF₄–LiF Salt Melts

temperature (°C)	SrCl ₂ –NaCl		ZrF ₄ –LiF	
	USPEX CN	expt. CN	USPEX CN	expt. CN
25	6.2	7.5 ± 1.3	6.8	8.0 ± 1.0
600	5.8	6.5 ± 1.9	6.3	6.2 ± 1.1
1000	5.6	5.8 ± 1.1	6.1	4.5 ± 2.5

Total agreement between XAS and USPEX data occurs when the USPEX fit overlaps with the processed XAS data. The fitted data are in near-total agreement with the experimentally determined spectra for Sr–Na–Cl, likely because the SrCl₂–NaCl phase diagram does not contain a ternary complex. Although the ZrF₄–LiF phase diagram is more complex, containing ternary compounds, the fit is in excellent agreement with the XAS data. This is probably because only the first coordination shell is considered in anticipation of complex ternary formation. The largest disagreement between the experiment and USPEX calculations occurs at 1000 °C, for which the salt melt contains Li₃ZrF₇, a compound that USPEX did not predict because it is a high-temperature phase. Comparison of the metal XAS backscattering distances to the first-shell M–X average distance for fitted USPEX Sr–Na–Cl and Zr–Li–F structures is shown in Table 4. The deviation between the experimental and computational distances are within the standard deviations. Overall, the agreement of our predicted average CNs and the fit of the most stable ternary

structures compared to XAS fitted values adds confidence to our approach toward predicting CNs in salt melts.

4. DISCUSSION

Our temperature-dependent CN distributions allowed us to reproduce trends and average CN values measured using EXAFS at elevated temperatures. Our predicted room-temperature CN of 6.2 for Sr–Na–Cl is within the calculated error limits for our companion EXAFS measurements that determined a value of 7.5 ± 1.3 for 5% SrCl₂–NaCl.²⁸ At 1000 °C, both calculated and measured CNs are in good agreement, having values of 5.6 and 5.8 ± 1.1, respectively. This also agrees with the values reported by McGreevy and Mitchell that showed Sr in SrCl₂ to have a CN of 6.9 at 925 °C, obtained using thermal neutron scattering,⁵⁶ as well as our predicted CN value of 6.61.

Because ZrF₄–LiF forms ternary compounds, it exhibits a more complex behavior than SrCl₂–NaCl. At room temperature, ZrF₄ crystallizes in a tetragonal structure with CN = 8, the same CN as that of the high-LiF-content compound Li₄ZrF₈. Considering 5% ZrF₄ in LiF, the equilibrium phases present at room temperature would be LiF and Li₄ZrF₈, forming Li₃ZrF₇ (unknown crystal structure) at >474 ± 5 °C.⁵⁷ The solidus of this composition is at 585 ± 5 °C and the liquidus is at 824 ± 5 °C.⁵⁸ Consequently, the expected CN for Zr is 8, which is in good agreement with our EXAFS measurement; however, the predicted CN of 6.8 is relatively low. At 1000 °C, the system is entirely melted, allowing Zr to form multiple complexes consisting of ZrF₆²⁻, ZrF₇³⁻, and

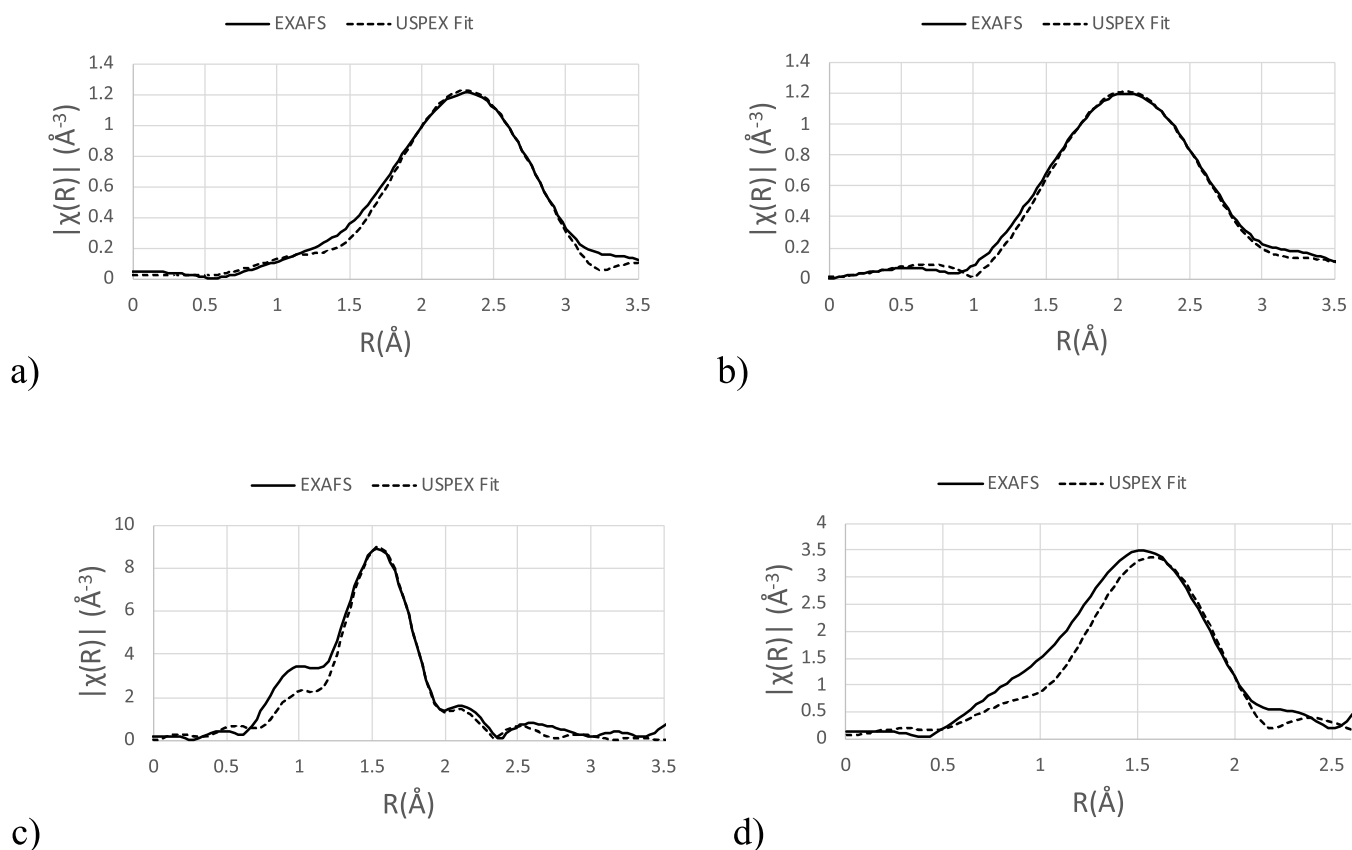


Figure 4. Comparison of raw EXAFS data with fitted EXAFS spectra for SrCl₂–NaCl (a,c) and ZrF₄–LiF (b,d) at 400 (a,c) and 1000 °C (b,d). Overlapping lines indicate the USPEX crystal structure matching well with EXAFS data. USPEX crystal structures are provided in the Supporting Information.

Table 4. Comparison of Experimental Metal Backscattering Distances to the Average Metal–Halide Distances (M–X) from USPEX Structures Used for Fitting in Figure 4

system	temp.(°C)	expt. M–X (Å)		calc. M–X (Å)	
SrCl ₂ –NaCl	400	2.94 ± 0.08		2.94 ± 0.12	
	1000	3.03 ± 0.01		2.94 ± 0.11	
ZrF ₄ –LiF	400	2.07 ± 0.02	2.23 ± 0.04	2.03 ± 0.02	2.18 ± 0.06
	1000	2.12 ± 0.04		2.09 ± 0.09	

ZrF₈⁴⁻ (CN = 6, 7, or 8, respectively).^{14,58} The computed CN of 6.1 at 1000 °C, however, is in relatively good agreement with the value of 7 predicted by Pauvert et al.¹⁴ using MD simulations at 50 K above the melting point (≈875 °C).

USPEX produced thousands of atomic configurations that represented well not only the lowest-energy solid structures but also structures that contained metal–halogen clusters in a large vacuum and single-metal atoms in highly concentrated alkali–halogen compositions. Our structural data set included many stoichiometric ratios similar to those used in MD calculations.^{12,59,60} Therefore, it is not surprising that our results diverged from experimental measurements of room-temperature solids because our method uses probabilistic averaging of multiple structures in order to replicate the varying CNs in liquid environments, while pure solids have well-defined CNs. EXAFS fits of our most stable USPEX crystal structures showed that they resemble the observed local structures, allowing us to gain insights into the first and second nearest neighbors in the melt. However, these salt melts can have multiple CNs at any given time that can be best sampled using molecular dynamics.

Our calculations for binary systems Sr–Cl and Zr–F and ternary systems Zr–Li–F and Sr–Na–Cl could reproduce the experimental thermodynamic convex hull, predicting the formation of the binary SrCl₂ and ZrF₄ phases as well as the ternary Li₄ZrF₈ and Li₃Zr₄F₁₉ phases. It did not predict the correct stoichiometry for ZrF₄, likely due to the limited number of atoms in a USPEX cell, which was less than the experimentally known unit cell of 40 atoms. It also had issues accurately predicting pure solid compounds, likely because of the high number of possible compositions that needed to be considered. In the future, seeding the algorithm with known crystal compositions may help. The calculations were, however, able to reproduce known trends in CN values with the metal content, decreasing as the metal atom fraction increased, and predict that these metals prefer a CN of 5 over 8. Overall, our study mirrors previous studies that have used USPEX to predict coordination environments such as that of Kheshti et al.,²⁶ who considered coordination environments of boron clusters. We therefore see no barriers to using our approach to investigate the coordination behavior of actinides in molten salt melts, following a similar study to that of Shields et al.¹⁷

5. CONCLUSIONS

We present here a computational study of CNs in two salt binary and ternary systems using the USPEX structure predictor algorithm coupled with the VASP electronic structure program. When compared to EXAFS experiments,²⁸ where appropriate, results for our ternary systems were found to closely model experimental observations and physical trends.

Our results reproduce known trends in Sr and Zr coordination with Cl and F as a function of the metal

composition and temperature, predicting the correct CNs as those shown in experiments for pure salt melts. Expanding our study to ternary systems, we were able to closely predict CNs as a function of temperature, which was observed in EXAFS measurements. The most stable predicted USPEX structures were used for fitting EXAFS data and was shown to have a small deviation, indicating that these artificial salt structures can be used to provide insights into the local structure of the melt. The verification of our approach allows us to continue our application of this genetic algorithm approach into more complex metallic salts such as uranium.

■ ASSOCIATED CONTENT

Supporting Information

The Supporting Information is available free of charge at <https://pubs.acs.org/doi/10.1021/acs.jpcc.2c00747>.

Na and Cl compositions for Sr–Na–Cl and Li and F compositions for Zr–Li–F (PDF)

■ AUTHOR INFORMATION

Corresponding Author

Theodore M. Besmann – Nuclear Engineering Program, University of South Carolina, Columbia, South Carolina 29208, United States; Email: BESMANN@cec.sc.edu

Authors

Matthew S. Christian – Nuclear Engineering Program, University of South Carolina, Columbia, South Carolina 29208, United States; orcid.org/0000-0002-3416-413X

Timothy J. Lynch – Department of Mechanical Engineering, University of Connecticut, Storrs, Connecticut 06369-3139, United States

Juliano Schorne-Pinto – Nuclear Engineering Program, University of South Carolina, Columbia, South Carolina 29208, United States; orcid.org/0000-0003-4208-4815

Amir M. Mofrad – Nuclear Engineering Program, University of South Carolina, Columbia, South Carolina 29208, United States

Nancy R. Birkner – Department of Materials Science and Engineering, Clemson University, Clemson, South Carolina 29634-0901, United States

Kyle S. Brinkman – Department of Materials Science and Engineering, Clemson University, Clemson, South Carolina 29634-0901, United States; orcid.org/0000-0002-2219-1253

Wilson K. S. Chiu – Department of Mechanical Engineering, University of Connecticut, Storrs, Connecticut 06369-3139, United States

Complete contact information is available at:

<https://pubs.acs.org/doi/10.1021/acs.jpcc.2c00747>

Notes

The authors declare no competing financial interest.

ACKNOWLEDGMENTS

The authors acknowledge the support from the Nuclear Energy University Program of the US Department of Energy Award ID: DE-NE0008772, 18-15065: "In Situ Measurement and Validation of Uranium Molten Salt Properties at Operationally Relevant Temperatures." The EXAFS measurements were carried out at the Stanford Synchrotron Radiation Lightsource, a national user facility operated by Stanford University on behalf of the U.S. Department of Energy, Office of Basic Energy Sciences. This work used the Extreme Science and Engineering Discovery Environment (XSEDE), which is supported by the National Science Foundation grant number ACI-1548562.

REFERENCES

- (1) Rao, C. J.; Ningshen, S.; Mallika, C.; Mudali, U. K. Molten Salt Corrosion Behavior of Structural Materials in LiCl-KCl-UCl₃ by Thermogravimetric Study. *J. Nucl. Matter* **2018**, *501*, 189–199.
- (2) Sun, H.; Wang, J.-Q.; Tang, Z.; Liu, Y.; Wang, C. Assessment of Effects of Mg Treatment on Corrosivity of Molten NaCl-KCl-MgCl₂ Salt with Raman and Infrared Spectra. *Corros. Sci.* **2020**, *164*, 108350.
- (3) Rollet, A.-L.; Salanne, M. Studies of the Local Structures of Molten Metal Halides. *Annu. Rep. Prog. Chem. Sect. C Phys. Chem.* **2011**, *107*, 88–123.
- (4) Bessada, C.; Rakhmatullin, A.; Rollet, A.-L.; Zanghi, D. High Temperature NMR Approach of Mixtures of Rare Earth and Alkali Fluorides: An Insight into the Local Structure. *J. Fluorine Chem.* **2009**, *130*, 45–52.
- (5) Rollet, A.-L.; Godier, S.; Bessada, C. High Temperature NMR Study of the Local Structure of Molten LaF₃-AF (A = Li, Na, K and Rb) Mixtures. *Phys. Chem. Chem. Phys.* **2008**, *10*, 3222–3228.
- (6) Machado, K.; Zanghi, D.; Sarou-Kanian, V.; Cadars, S.; Burbano, M.; Salanne, M.; Bessada, C. Study of NaF-AlF₃ Melts by Coupling Molecular Dynamics, Density Functional Theory, and NMR Measurements. *J. Phys. Chem. C* **2017**, *121*, 10289–10297.
- (7) Dracopoulos, V.; Vagelatos, J.; Papatheodorou, G. N. Raman Spectroscopic Studies of Molten ZrF₄-KF Mixtures and of A₂ZrF₆, A₃ZrF₇ (A = Li, K or Cs) Compounds. *J. Chem. Soc., Dalton Trans.* **2001**, *7*, 1117–1122.
- (8) Pauvert, O.; Zanghi, D.; Salanne, M.; Simon, C.; Rakhmatullin, A.; Matsuura, H.; Okamoto, Y.; Vivet, F.; Bessada, C. In Situ Experimental Evidence for a Nonmonotonous Structural Evolution with Composition in the Molten LiF-ZrF₄ System. *J. Phys. Chem. B* **2010**, *114*, 6472–6479.
- (9) Gill, S. K.; Huang, J.; Mausz, J.; Gakhar, R.; Roy, S.; Vila, F.; Topsakal, M.; Phillips, W. C.; Layne, B.; Mahurin, S.; et al. Connections between the Speciation and Solubility of Ni(II) and Co(II) in Molten ZnCl₂. *J. Phys. Chem. B* **2020**, *124*, 1253–1258.
- (10) Bessada, C.; Zanghi, D.; Salanne, M.; Gil-Martin, A.; Gibilaro, M.; Chamelot, P.; Massot, L.; Nezu, A.; Matsuura, H. Investigation of Ionic Local Structure in Molten Salt Fast Reactor LiF-ThF₄-UF₄ Fuel by EXAFS Experiments and Molecular Dynamics Simulations. *J. Mol. Liq.* **2020**, *307*, 112927.
- (11) Sun, J.; Guo, X.; Zhou, J.; Dai, J.; Song, S.; Bao, H.; Lin, J.; Yu, H.; He, S.; Jiang, F.; et al. Investigation of the Local Structure of Molten ThF₄-LiF and ThF₄-LiF-BeF₂ Mixtures by High-Temperature X-Ray Absorption Spectroscopy and Molecular-Dynamics Simulation. *J. Synchrotron Radiat.* **2019**, *26*, 1733–1741.
- (12) Ocadiz-Flores, J. A.; Gheribi, A. E.; Vlieland, J.; de Haas, D.; Dardenne, K.; Rothe, J.; Konings, R. J. M.; Smith, A. L. Examination of the Short-Range Structure of Molten Salts: ThF₄, UF₄, and Related Alkali Actinide Fluoride Systems. *Phys. Chem. Chem. Phys.* **2021**, *23*, 11091–11103.
- (13) Okamoto, Y. XAFS Simulation of Highly Disordered Materials. *Nucl. Instrum. Methods Phys. Res. Sect. A Accel. Spectrom. Detect. Assoc. Equip.* **2004**, *526*, 572–583.
- (14) Pauvert, O.; Salanne, M.; Zanghi, D.; Simon, C.; Reguer, S.; Thiaudière, D.; Okamoto, Y.; Matsuura, H.; Bessada, C. Ion Specific Effects on the Structure of Molten AF-ZrF₄ Systems (A⁺ = Li⁺, Na⁺, and K). *J. Phys. Chem. B* **2011**, *115*, 9160–9167.
- (15) Glass, C. W.; Oganov, A. R.; Hansen, N. USPEX-Evolutionary Crystal Structure Prediction. *Comput. Phys. Commun.* **2006**, *175*, 713–720.
- (16) Lyakhov, A. O.; Oganov, A. R.; Stokes, H. T.; Zhu, Q. New Developments in Evolutionary Structure Prediction Algorithm USPEX. *Comput. Phys. Commun.* **2013**, *184*, 1172–1182.
- (17) Shields, A. E.; Miskowicz, A. J.; Maheshwari, K.; Kirkegaard, M. C.; Staros, D. J.; Niedziela, J. L.; Kapsimalis, R. J.; Anderson, B. B. The Impact of Coordination Environment on the Thermodynamic Stability of Uranium Oxides. *J. Phys. Chem. C* **2019**, *123*, 15985–15995.
- (18) Lopes, D. A.; Kocevski, V.; Wilson, T. L.; Moore, E. E.; Besmann, T. M. Stability of U₃Si₄ Phase in U-Si System: Crystal Structure Prediction and Phonon Properties Using First-Principles Calculations. *J. Nucl. Matter.* **2018**, *510*, 331–336.
- (19) Wu, S. Q.; Ji, M.; Wang, C. Z.; Nguyen, M. C.; Zhao, X.; Umamoto, K.; Wentzcovitch, R. M.; Ho, K. M. An Adaptive Genetic Algorithm for Crystal Structure Prediction. *J. Phys. Condens. Matter* **2014**, *26*, 035402.
- (20) Paszkowicz, W. Genetic Algorithms, a Nature-Inspired Tool: Survey of Applications in Materials Science and Related Fields. *Mater. Manuf. Processes* **2009**, *24*, 174–197.
- (21) Kirklın, S.; Saal, J. E.; Hegde, V. I.; Wolverton, C. High-Throughput Computational Search for Strengthening Precipitates in Alloys. *Acta Mater.* **2016**, *102*, 125–135.
- (22) Baturin, V. S.; Lepeshkin, S. V.; Matsko, N. L.; Oganov, A. R.; Uspenskii, Y. A. Prediction of the Atomic Structure and Stability for the Ensemble of Silicon Nanoclusters Passivated by Hydrogen. *Europhys. Lett.* **2014**, *106*, 37002.
- (23) Sharma, T.; Sharma, R.; Kanhere, D. G. A DFT Study of Se_nTe_n Clusters. *Nanoscale Adv.* **2022**, *4*, 1464–1482.
- (24) Mitra, S.; Chattopadhyay, R.; Pal, M.; Das, G. P.; Bhadra, S. K. First Principles Study of Ag Adsorption Mechanism in Amorphous Large Silica Clusters. *Phys. E* **2019**, *112*, 26–35.
- (25) Sharma, T.; Sharma, R.; Tamboli, R. A.; Kanhere, D. G. Ab Initio Investigation of Structural and Electronic Properties of Selenium and Tellurium Clusters. *Eur. Phys. J. B* **2019**, *92*, 51.
- (26) Kheshti, T.; Mahdavi, Z.; Noorzadeh, S. Umbrella-Shaped vs Planar; Evolutionary Search for BnQ, Be@BnQ (n = 6–12, Q = 0, –1) Clusters. *J. Mol. Liq.* **2021**, *328*, 115389.
- (27) Mahdavi, Z.; Shojaei, F. Evolutionary Search for (M@B16): Q (M = Sc-Ni; Q = 0/-1) Clusters: Bowl/Boat vs. Tubular Shape. *Phys. Chem. Chem. Phys.* **2019**, *21*, 22618–22628.
- (28) Lynch, T. J.; Birkner, N. R.; Christian, M. S.; Wrubel, J. A.; Schorne-Pinto, J.; van Veelan, A.; Bargar, J. R.; Besmann, T. M.; Brinkman, K. S.; Chiu, W. K. S. In Situ Determination of Speciation and Local Structure of NaCl-SrCl₂ and LiF-ZrF₄ Molten Salts. *J. Phys. Chem. B* **2022**, *126*, 1539–1550.
- (29) Blöchl, P. E. Projector Augmented-Wave Method. *Phys. Rev. B* **1994**, *50*, 17953–17979.
- (30) Kresse, G.; Joubert, D. From Ultrasoft Pseudopotentials to the Projector Augmented-Wave Method. *Phys. Rev. B* **1999**, *59*, 1758–1775.
- (31) Kresse, G.; Furthmüller, J. Efficient Iterative Schemes for Ab Initio Total-Energy Calculations Using a Plane-Wave Basis Set. *Phys. Rev. B* **1996**, *54*, 11169–11186.
- (32) Kresse, G.; Hafner, J. Ab Initio Molecular-Dynamics Simulation of the Liquid-Metalamorphous-Semiconductor Transition in Germanium. *Phys. Rev. B* **1994**, *49*, 14251–14269.
- (33) Kresse, G.; Hafner, J. Ab Initio Molecular Dynamics for Liquid Metals. *Phys. Rev. B* **1993**, *47*, 558–561.
- (34) Perdew, J. P.; Burke, K.; Ernzerhof, M.; of Physics, D. Quantum Theory Group Tulane University, N. O. L. 70118 J. Generalized Gradient Approximation Made Simple. *Phys. Rev. Lett.* **1996**, *77*, 3865–3868.

- (35) Liu, X.-Y.; Andersson, D. A. Revisiting the Diffusion Mechanism of Helium in UO_2 : A DFT+U Study. *J. Nucl. Mater.* **2018**, *498*, 373–377.
- (36) Liu, X.-Y.; Andersson, D. A.; Uberuaga, B. P. First-Principles DFT Modeling of Nuclear Fuel Materials. *J. Mater. Sci.* **2012**, *47*, 7367–7384.
- (37) Marzari, N.; Vanderbilt, D.; de Vita, A.; Payne, M. C. Thermal Contraction and Disorder of the Al(110) Surface. *Phys. Rev. Lett.* **1999**, *82*, 3296–3299.
- (38) Grimme, S.; Antony, J.; Ehrlich, S.; Krieg, H. A Consistent and Accurate Ab Initio Parametrization of Density Functional Dispersion Correction (DFT-D) for the 94 Elements H-Pu. *J. Chem. Phys.* **2010**, *132*, 154104.
- (39) Christian, M. S.; Johnson, E. R.; Besmann, T. M. Interplay between London Dispersion, Hubbard U, and Metastable States for Uranium Compounds. *J. Phys. Chem. A* **2021**, *125*, 2791–2799.
- (40) Vogel, S. C.; Andersson, D. A.; Monreal, M. J.; Jackson, J. M.; Parker, S. S.; Wang, G.; Yang, P.; Zhang, J. Crystal Structure Evolution of UCl_3 from Room Temperature to Melting. *JOM* **2021**, *73*, 3555–3563.
- (41) Otero-De-La-Roza, A.; Johnson, E. R.; Luaña, V. Critic2: A Program for Real-Space Analysis of Quantum Chemical Interactions in Solids. *Comput. Phys. Commun.* **2014**, *185*, 1007–1018.
- (42) Kirklin, S.; Saal, J. E.; Meredig, B.; Thompson, A.; Doak, J. W.; Aykol, M.; Rühl, S.; Wolverton, C. The Open Quantum Materials Database (OQMD): Assessing the Accuracy of DFT Formation Energies. *npj Comput. Mater.* **2015**, *1*, 15010.
- (43) Wang, B.; Xia, C.-J.; Fang, H.-L.; Chen, W.-J.; Zhang, Y.-F.; Huang, X. Mononuclear Thorium Halide Clusters ThX_4 (X = F, Cl): Gas-Phase Hydrolysis Reactions. *Phys. Chem. Chem. Phys.* **2018**, *20*, 21184–21193.
- (44) Jacob, F.; Pogrebnoi, A. M.; Pogrebnyaya, T. P. Cluster Ions in Saturated Vapor over Barium Difluoride: Structure and Thermodynamic Properties. *Comput. Theor. Chem.* **2016**, *1091*, 137–149.
- (45) Rabilloud, F. Structure and Stability of Coinage Metal Fluoride and Chloride Clusters (M_NF_n and M_NCl_n , M = Cu, Ag, or Au; N = 1–6). *J. Comput. Chem.* **2012**, *33*, 2083–2091.
- (46) Kuc, A.; Heine, T.; Mineva, T. Niobium-Chloride Octahedral Clusters as Building Units for Larger Frameworks. *Struct. Chem.* **2012**, *23*, 1357–1367.
- (47) Rabilloud, F.; Mathian, D. Ab Initio Study of Neutral and Charged Copper Bromide (CuBr_n) Clusters (n = 1–6). *J. Cluster Sci.* **2012**, *23*, 165–176.
- (48) Ravel, B.; Newville, M. ATHENA, ARTEMIS, HEPHAESTUS: Data Analysis for X-Ray Absorption Spectroscopy Using IFEFFIT. *J. Synchrotron Radiat.* **2005**, *12*, 537–541.
- (49) Stern, E. A. Number of Relevant Independent Points in X-Ray-Absorption Fine-Structure Spectra. *Phys. Rev. B: Condens. Matter Mater. Phys.* **1993**, *48*, 9825.
- (50) Downward, L.; Booth, C. H.; Lukens, W. W.; Bridges, F. A Variation of the F-Test for Determining Statistical Relevance of Particular Parameters in EXAFS Fits. *AIP Conf. Proc.* **2007**, *882*, 129–131.
- (51) Okamoto, Y.; Yaita, T.; Minato, K. High-Temperature XAFS Study of Solid and Molten SrCl_2 . *J. Non-Cryst. Solids* **2004**, *333*, 182–186.
- (52) Papiernik, R.; Mercurio, D.; Frit, B. Structure du Tetrafluorure de Zirconium, ZrF_4 . *Acta Crystallogr., Sect. A: Cryst. Phys., Diff., Theor. Gen. Crystallogr.* **1982**, *38*, 2347–2353.
- (53) Legein, C.; Fayon, F.; Martineau, C.; Body, M.; Buzaré, J.-Y.; Massiot, D.; Durand, E.; Tressaud, A.; Demourgues, A.; Péron, O.; et al. 19F High Magnetic Field NMR Study of β - ZrF_4 and CeF_4 : From Spectra Reconstruction to Correlation between Fluorine Sites and 19F Isotropic Chemical Shifts. *Inorg. Chem.* **2006**, *45*, 10636–10641.
- (54) Maksoud, L.; Gobet, M.; Zanghi, D.; Matsuura, H.; Numakura, M.; Pauvert, O.; Bessada, C. NMR and EXAFS Investigations of Lanthanum Fluoride Solubility in Molten $\text{LiF-ZrF}_4\text{-LaF}_3$ Mixture: Application in Molten Salts Reactor. *Molten Salts Chem. Technol.* **2014**, 403–409.
- (55) Sidorov, L. N.; Karasev, N. M.; Korenev, Y. M. Mass-Spectrometric Study of (Potassium Fluoride+Zirconium Tetrafluoride) and (Caesium Fluoride+Zirconium Tetrafluoride). Molecular Composition of Vapour. Activities. Congruent and Incongruent Sublimation of $3\text{KF}\cdot\text{ZrF}_4$ Crystal. *J. Chem. Thermodyn.* **1981**, *13*, 915–935.
- (56) McGreevy, R. L.; Mitchell, E. W. J. The Determination of the Partial Pair Distribution Functions for Molten Strontium Chloride. *J. Phys. C: Solid State Phys.* **1982**, *15*, 5537–5550.
- (57) Novoselova, A. V.; Korenev, Y. M.; Simanov, Y. P. Research on the System LiF-ZrF_4 . *Dokl. Akad. Nauk SSSR* **1961**, *139*, 892–894.
- (58) Ard, J.; Johnson, K.; Christian, M.; Schorne Pinto, J.; Yingling, J.; Besmann, T.; McMurray, J.; Peng, J. *FY20 Status Report on the Molten Salt Thermodynamic Database (MSTDB) Development*, 2020. No. September.
- (59) Bessada, C.; Pauvert, O.; Zanghi, D.; Rollet, A. L.; Saroukhanian, V.; Gobet, M.; Moussaed, G.; Rakhmatullin, A.; Salanne, M.; Simon, C.; Matsuura, H. In Situ Experimental Approach of the Speciation in Molten Lanthanide and Actinide Fluorides Combining NMR, EXAFS and Molecular Dynamics. *ECS Trans.* **2010**, *33*, 361–369.
- (60) Li, X.; Song, J.; Shi, S.; Yan, L.; Zhang, Z.; Jiang, T.; Peng, S. Dynamic Fluctuation of U^{3+} Coordination Structure in the Molten LiCl-KCl Eutectic via First Principles Molecular Dynamics Simulations. *J. Phys. Chem. A* **2017**, *121*, 571–578.